Natural Hazards (2026) 122:610
https://doi.org/10.1007/s11069-026-08389-y

ORIGINAL PAPER

Lithological, geomorphological and tectonic control on landslide processes in Southern Italy: insights from a regional inventory and metrics of landscape evolution

Dario Gioia[1] · Giuseppe Corrado[2,3] · Lucia Contillo[2] · Antonio Minervino Amodio[1] · Marcello Schiattarella[2]

Received: 15 January 2026 / Accepted: 11 August 2026 / Published online: 24 August 2026

Abstract
The landscape of Southern Italy is widely affected by landslide processes of different types, sizes and ages, which locally play an important role in the landscape evolution, slope evolution, and sediment mobility of different sectors of the belt. We perform a statistical analysis of a landslide inventory map that covers the administrative territory of Basilicata, southern Italy, aimed at the investigation of the interplay between landslide distribution and lithological and geomorphological factors. Statistical analysis of the landslide inventory map and the comparison with geothematic maps and landscape metrics provide new insights into both the main predisposing factors of landslide processes and the role of long-term morphotectonic evolution on the landslide pattern. Our results indicate a total landslide density of about 7% across the study area, with a predominance of slow-moving landslides and a highly clustered, non-random spatial distribution. Landslide-dominated landscapes, characterized by the superimposition of large deep-seated and smaller, shallow landslides, are also widespread. Analysis of the relationships between landslide patterns and metrics of landscape evolution indicates that lithological and topographic characteristics alone cannot account for the preferential occurrence of landslides in these morphotectonic domains, pointing instead to a significant role of tectonically induced landscape disequilibrium in controlling landslide distribution.

Keywords Landslide inventory · Tectonic uplift · Landslide hazard · Southern Italy

✉ Dario Gioia
dario.gioia@cnr.it

1 Consiglio Nazionale delle Ricerche, ISPC, Tito Scalo, Potenza, Italy

2 Università della Basilicata, DIUSS, Matera, Italy

3 Università degli Studi di Napoli "Parthenope", DIST, Naples, Italy

1 Introduction

Landsliding exerts a relevant role in landscape evolution, representing a dominant geomorphic process in many tectonically-active mountain belts (Cendrero and Dramis 1996; Korup et al. 2010). Nevertheless the importance of landslide processes in the geomorphological evolution of high-relief and fast uplifting areas (Korup et al. 2010; Roering et al. 2015), landslide research is frequently focused on the surface and subsurface characterization of a single landslide or on catchment-scale analyses of the spatial distribution of landslide processes to identify their predisposing factors and/or delineate susceptibility maps. This hazard- and risk-oriented perspective of landslide studies tends to understate the increasingly recognised link between the dynamic state of landscapes – driven by tectonic and/or climate perturbations – and landslide distribution (Kashyap and Behera 2023; Korup et al. 2010; Ouimet et al. 2007; Roering et al. 2015). Indeed, several recent studies demonstrated a positive correlation between uplift rates and landslide distribution (Aristizábal and Korup 2025; Bian et al. 2025; Delchiaro et al. 2023; Kashyap and Behera 2023), suggesting that spatial and temporal landslide pattern can be predicted by the analysis of catchment-scale perturbations induced by tectonic and climatic drivers.

In Southern Italy, the landscape is largely affected by landslide processes of different types, sizes and ages, which locally play an important role in the landscape evolution, slope processes, and sediment mobility across different sectors of the belt. Numerous landslide studies are widespread in this mountain belt, although they are mainly focused on the subsurface characterization of slow-moving or complex landslides (Bentivenga et al. 2019; Calcaterra et al. 2012; Conforti et al. 2021; Di Maio et al. 2018; Gioia et al. 2024a; Perrone et al. 2021; Spalluto et al. 2021) or on the compilation of landslide inventory maps (LIMs) at a catchment scale (Ardizzone et al. 2023; Bentivenga et al. 2023; Bucci et al. 2021; Conforti et al. 2013, 2015; Lazzari and Gioia 2016; Santangelo et al. 2013, 2014). Small-scale investigations often provide a well-constrained picture of geometry, features, kinematics, and controlling factors of the most impressive landslides of the mountain belt, whereas LIMs analysis supports the reconstruction of the spatial distribution and type of the landslide phenomena and the identification of their main predisposing factors. These studies can be valuable for assessing local predisposing and triggering factors or for producing sub-regional susceptibility and hazard maps, but they are not well suited to a synoptic characterization of the contribution of landslides to landscape evolution in active mountain belts. Indeed, previous works in the southern Italian belt have overlooked the potential role of tectonic uplift and landscape disequilibrium on landslide occurrence, despite modern views emphasized strong relationships between catchment-scale tectonic perturbations and spatial distribution of landslide processes. In general, highly-perturbed catchments exhibiting high local relief, high integral hypsometric and ksn-values show higher density of landslides, although a different response of shallower and deep-seated landslides was commonly observed (Aristizábal and Korup 2025; Bian et al. 2025; Delchiaro et al. 2023; Discienza et al., 2023; Gallen et al. 2011; Korup et al. 2010; Liu et al. 2015; Ouimet et al. 2007).

This study presents a statistical analysis of a geomorphological LIM covering a large sector of the southern Apennine belt, Italy (Fig. 1) aimed at the investigation of the interplay among landslide distribution, lithology, and geomorphological features. The landslide dataset integrates and updates the information provided by Lazzari et al. (2018). The availability of a large-scale and homogeneous geomorphological LIM allowed us to perform a compre-

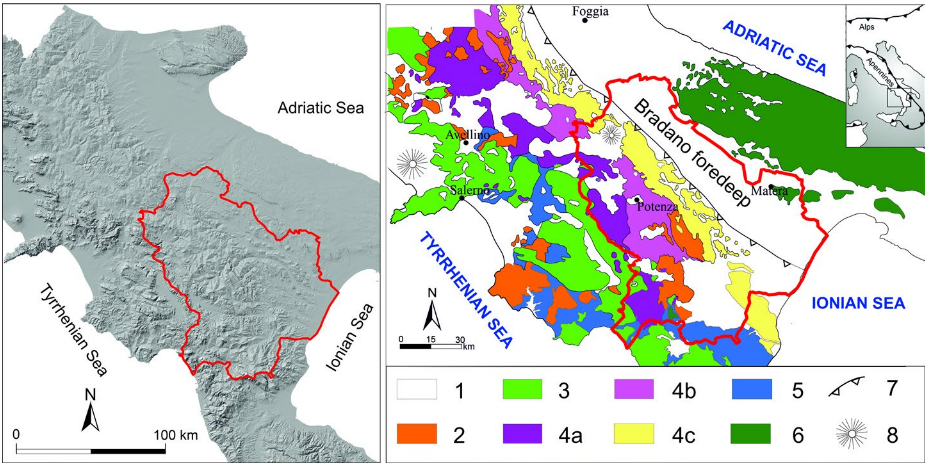

Fig. 1 Geographical and geological setting of the study area. Legend of the geological sketch map of southern Italy (mod. after Schiattarella et al. 2017): 1. Pliocene to Quaternary clastics and Quaternary volcanics; 2. Miocene syntectonic deposits; 3) Mesozoic-Cenozoic Apennine carbonate platform units; 4) Mesozoic-Cenozoic Lagonegro basinal units: 4a Lower-middle Triassic to Miocene shallow-water and deep-sea succession of the Lagonegro-type Monte Arioso unit; 4b) Lower-middle Triassic to Miocene shallow-water and deep-sea succession of the Lagonegro-type Groppa d'Anzi unit; 4c) Cretaceous to Miocene deep-sea succession of the Lagonegro-type Campomaggiore unit; 5 Cretaceous to Oligocene ophiolite-bearing internal units (Ligurian units); 6 Mesozoic-Cenozoic Apulian carbonate platform units; 7). Thrust front of the chain. 8). Volcano

hensive investigation of the spatial distribution of the landslide processes at a regional scale and to infer the influence of geological and geomorphological factors on slope (un)stability. To infer the main geological and geomorphological predisposing factors of the landslide distribution, we use a traditional approach based on statistical analyses of the LIM and its correlation with geo-thematic maps. Such investigations highlighted that the preferential distribution of landslide processes of the study area can be only partially explained by litho-structural setting. Hence, we explored the potential role of tectonics and fluvial incision on landslide processes by comparing landslide pattern with metrics that describe the dynamic state and evolution of the landscape.

2 Geological, morphotectonic and climate setting

The southern Apennine (Fig. 1) is a fold-and-thrust belt with a general NE vergence, that developed, since the late Oligocene, at the top of the subducting Apulia foreland. The belt includes tectonic units of the western border of the Apulian plate, consisting of Mesozoic-Cenozoic shallow-water and deep-sea sedimentary rocks (Menardi Noguera and Rea 2000). Miocene to Pliocene evolution of the belt is largely featured by thrusting and NE migration of both Mesozoic-Cenozoic tectonic units and Neogene–Pleistocene foredeep deposits, which are progressively and diachronically involved in the contractional structure from easternmost sectors to western ones (Pescatore et al. 1999). Starting from the Lower Pliocene, several thrust-top basins (i.e. the Ariano Irpino, Ofanto, Potenza, Calvello and Sant'Arcangelo) were formed (Ascione et al.,2012). They are arranged along a roughly

NNO-SSW orientation in the outer zone of the belt. During the Quaternary, the contractional structure was largely affected by strike-slip and normal high-angle faults, which promoted the relief increase and the development of several tectonic basins, especially in the axial and inner zones of the chain (Gioia et al. 2023; Schiattarella et al. 2003; Ascione et al. 2013; Valente et al. 2019).

Such a complex geological and tectonic evolution strongly influenced the geomorphological setting and the spatial distribution of the main landforms of the chain. From SW to NE, the landscape shows a well-defined zonation into domains with similar tectono-stratigraphic and morphotectonic features (Schiattarella et al. 2017). More specifically, five different domains can be recognized (Fig. 2), which exhibit similar characters in terms of distribution of the main geological units, landscape features, and morphotectonic evolution. Such features strongly influenced landscape elements, drainage network pattern, and slope failure processes (Schiattarella et al. 2024).

The inner or Tyrrhenian zone of the southern Apennines shows an articulated morpho-structural arrangement due to the differential uplift along WNW-ESE and NE-SW-trending high-angle and listric faults. Pliocene to Quaternary fault activity promoted both the uplift of impressive carbonate ridges and the formation of several tectonically-controlled coastal plains (Corrado et al. 2025). Narrow pocket beaches locally occur in embayments of high-relief and rocky coasts.

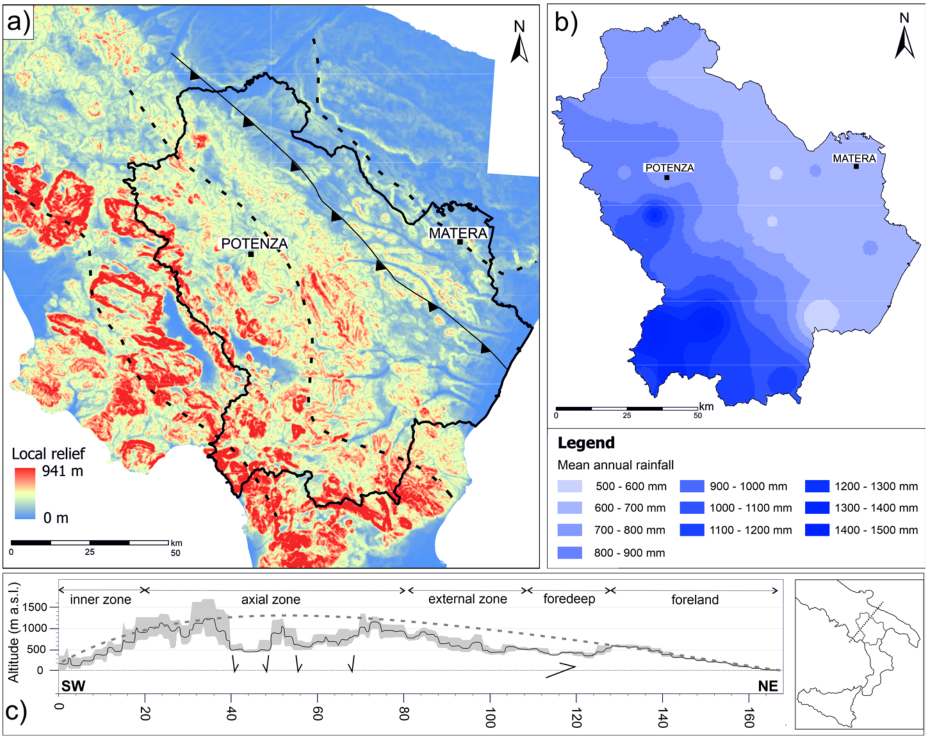

Fig. 2 Relief map (**a**), circular windows: 500 m, mean annual rainfall (**b**), period: 2014–2024 and swath profile (**c**) of the study area. Relief map and swath profile depict the boundaries of the main morphotectonic domains of the study area (from SW to NE: inner zone, axial zone, outer zone, foredeep and foreland)

The axial zone of the chain is featured by an alternation of impressive fault-related mountain ridges and tectonic basins. This sector coincides with the seismogenic belt of the southern Apennines (Ascione et al. 2013), where stronger historical earthquakes have occurred along WNW-ESE-trending high-angle normal faults (Cocco et al. 1993). The landscape is characterized by the greatest relief, and positive morphostructures are mainly developed in Mesozoic shallow-water carbonate of the Apennine carbonate platform unit and coeval deep-sea sedimentary rocks of the Lagonegro Tectonic Units (see Schiattarella et al. 2024). A further distinctive feature of these morphostructures is the presence of a staircase of subhorizontal erosional surfaces, which developed between about 500 and 2000 m a.s.l. above the present-day thalwegs and represent the remnants of a late Pliocene planation surface, strongly dislocated by fault activity (Schiattarella et al. 2017 and references therein). Quaternary fault activity and related base-level lowering promoted the relief increase of the uplifted blocks and the creation of accommodation space for the development of several tectonic depressions. The infill of these tectonic basins is generally made of Quaternary continental clastic deposits, although Pliocene marine deposits can be locally observed (Schiattarella et al. 2003).

The gentler landscape of the outer/front zone of the chain is featured by NNW-SSE-trending thrust sheets and monoclinal ridges, which are generally carved in Numidian sandstones and Cretaceous to Miocene basinal and clay-rich deposits (Pescatore et al. 1999 and references therein). Landforms in thrust-top basins are typically represented by gently-dipping hillslopes, which represent monoclinal ridges in Miocene syntectonic units and Pliocene clastic deposits. They are deeply incised by the main rivers flowing into the Ionian Sea.

The hilly landscape of the northernmost and easternmost sectors of the study area developed into Lower Pleistocene marine foredeep deposits. These sectors are largely affected by badlands and shallow landslides. As a result of the gradual emersion of the foredeep area since the Middle Pleistocene, marine foredeep deposits passed upward to continental and coarser-grained clastic deposits. In these sectors, flat-topped landforms or terraced marine surfaces developed (Gioia et al. 2024b; Schiattarella et al. 2024).

Uplift rates are irregularly distributed in the study area. Higher values of about 0.6 mm/yr occurred in the axial zone of the chain, as a result of the Quaternary uplift and block-faulting activity (Schiattarella et al. 2017 and references therein).

From a climate viewpoint, the study area shows a typical temperate and hot-summer Mediterranean climate. Mean annual precipitation ranges from about 500 mm to 1500 mm, with a clear linear correlation between the increase of the mean annual rainfall and the elevation of the landscape (Fig. 2). Seasonal distribution of the precipitation has a high variability and it is featured by dry periods and short-term (i.e.: two or three days) severe rainfall events. Such heavy events generally occurred in autumn and spring.

3 Methodology

The landslide dataset analyzed here was prepared from a Landslide Inventory Map (LIM) compiled in the frame of a national project of landslide mapping (Lazzari et al. 2018). The mapping was originally carried out at a 1:10,000 scale according to standard rules and procedures of the IFFI project (the Inventory of Landslide Phenomena in Italy), which largely follows consolidated preparation techniques of a geomorphological landslide inventory (*sensu* Guzzetti et al. 2012). The inventory covers the territory of about 8000 km^2 of the Basilicata region and was updated here using recent orthophotos and satellite images.

Recently, our research group prepared a detailed map of the geolithological and landscape units of the Basilicata region (Schiattarella et al. 2024). These cartographic products were used to support the GIS-aided statistical analyses of the relationships between geological and geomorphological factors and the spatial distribution of the landslides.

We used an airborne LIDAR DEM with a resolution of 5 m for terrain analysis of the Basilicata region for landform analysis, extraction of DEM-derivatives, and statistical analysis. The derivation of some landscape metrics such as the χ and Local Relief maps required a DEM at a larger scale than the territory of the Basilicata region: in this case, we use the 10-m Tinitaly DEM (Tarquini et al. 2012).

To investigate the possible control of late Quaternary surface uplift on landslide pattern, we derive two landscape metrics related to the stream power model (Whipple 2004): the normalized channel steepness index (ksn, Whipple 2004) and the χ metric (Perron and Royden 2013). The metrics provide an estimate of the transient state or the degree of tectonic perturbations of a landscape, providing insights on the role of tectonic activity and fluvial incision on the spatial distribution of mapped landslides.

3.1 Landslide inventory

The LIM was derived from an accurate revision of the IFFI dataset, which has been prepared following standardized procedures and rules (see Lazzari et al. 2018 and Trigila et al. 2010 for some more details on the LIM preparation). The classification of the landslides uses the scheme and criteria introduced by Cruden and Varnes (1996) and WP/WLI (1993), with some minor modifications (Hungr et al. 2014).

Detection, mapping, and classification of landslides at a detailed scale (i.e.:1:10,000) were performed by using well-consolidated and widely-used geomorphological techniques, based on multitemporal photo-interpretation and focused field survey. More specifically, we interpret digital stereoscopic aerial-photos (years: 1954, 1990 and 2003, scale 1:33,000; 1974, scale 1:16,000; source: Italian Military Geographic Institute IGMI), and high-resolution aerial orthophotos (years: 2008, 2013, 2017; source: Italian Ministry of Agriculture).

We updated the original inventory by integrating it with the photo-interpretation of more recent images (i.e.: 2023 orthophotos at a 0.2 m resolution and recent Google Earth satellite images). Apart from a significant improvement in terms of mapping and classification of the original landslide dataset, our revision includes an additional classification of the landslide inventory, which has been proven as an effective approach to capture different geomorphic stages of tectonic influence on landslide pattern (Aristizábal and Korup 2025). Accordingly, we divided the landslides of the LIM into two different classes, which are related to the relative age and importance for the landscape evolution. More specifically, the two classes are the following: larger, deeper and older landslides (hereafter DLL) and smaller, shallower, and younger ones (LDD).

The DLL class includes deep-seated landslides with an inferred age older than the images in the cartographic sources. Locally, they show typical features of relict landslides but often remain well-preserved or large enough to have clearly defined head scarps and bodies (Fig. 3). Their geomorphic features indicate a relevant role in the long-term landscape evolution of the study area.

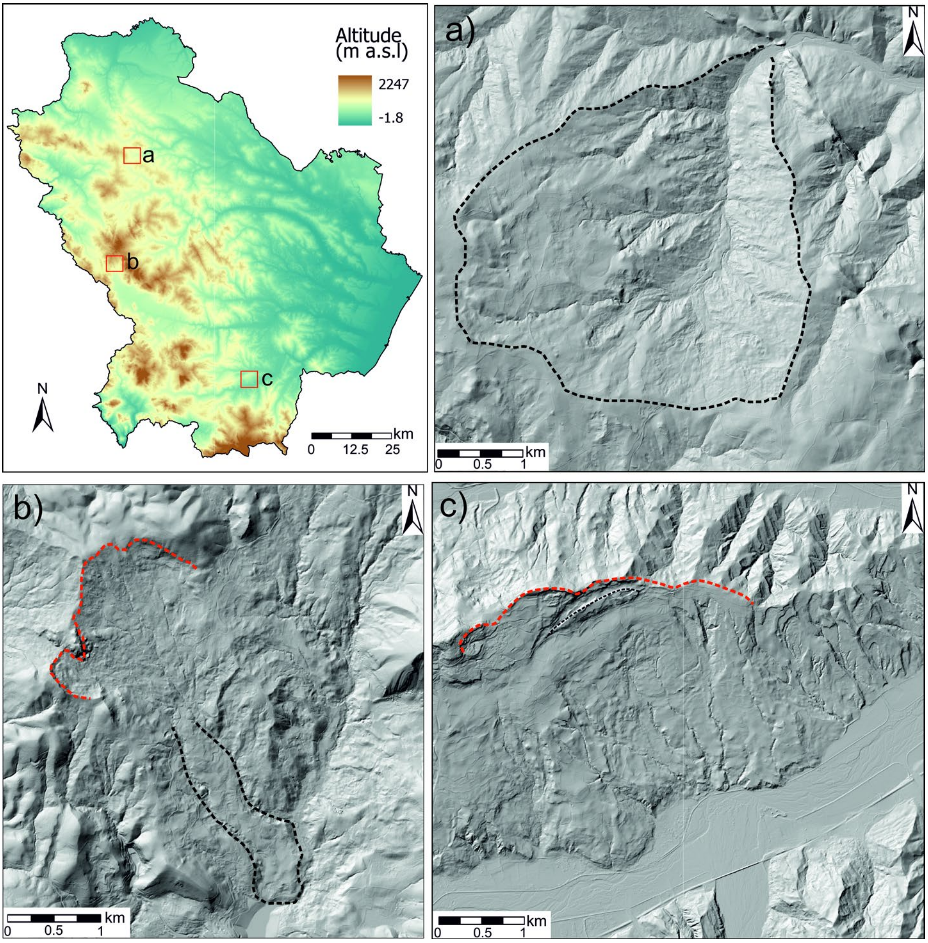

Fig. 3 Examples of landslide-dominated landscapes of the study area. **a** roughly-circular catchment at the front of the chain (about 10 km to the NE from the Potenza city) featured by complex superimposition of landslides of different size, type, depth, and age; **b** Huge roto-translational slide evolving into earthflow in the axial zone of the chain (Pietra Maura landslide, see Bentivenga et al. 2026). Dashed red line outlines the main degraded scarp, whereas the black one indicated the large and incised toe. **c** Deep-Seated Gravitational Slope Deformation along the left-orographic side of the upper reach of the Sinni River. Red and black dashed lines outline the main scarp and a trench, respectively

3.2 Landscape metrics related to the stream power model

To test the influence of tectonic activity and related fluvial incision on landslide distribution, we estimated DEM derivatives and landscape metrics that are linked to the degree of tectonic perturbation of a landscape.

The relief of the study area (Fig. 2) was extracted by using a circular moving window of 500 m over the 10-m DEM. A measure of the degree of the stage of maturity and geomorphological disequilibrium of the catchment was provided by the hypsometric integrals (HI), which were extracted using the WhiteToolBox (Lindsay 2016).

We use Topotoolbox suite (Schwanghart and Scherler 2014) to derive the drainage network, catchments, longitudinal profiles, and landscape metrics related to the Stream Power Incision Model (SPIM, Whipple and Tucker 1999). Through a visual comparison with permanent channels of official topographic maps at a 1:10,000 scale, we estimated a minimum accumulation threshold area of 60,000 m^2 to delineate the drainage network of the study area. SPIM expressed the detachment-limited river incision E as a power-law of the drainage area (A) and the channel slope (S), scaled by a constant K (the erodibility coefficient):

$$\mathrm{E} = \mathrm{K}\ \mathrm{A}^{\mathrm{m}}\mathrm{S}^{\mathrm{n}} \tag{1}$$

the exponents m and n are empirical constants (Lague 2014), whereas K depends by lithology, climate and channel geometry.

Under steady-state conditions (U=E), Eq. 1 can be re-write as follows:

$$\mathrm{S} = \left(\frac{U}{K}\right)^{\frac{1}{n}} A^{-\frac{m}{n}} \tag{2}$$

The Eq. 2 has the same form of the well-known empirical Flint's law:

$$\mathrm{S} = \mathrm{Ks}\ A^{-\theta} \tag{3}$$

where Ks represents the channel steepness index and m/n or θ is the concavity index.

Using a best-fit θ_{ref}, the normalized steepness index ksn, can be expressed as:

$$\mathrm{Ksn} = \mathrm{S}\ \mathrm{A}^{-\theta} \tag{4}$$

where best-fit θ is routinely estimated by a regression procedure on a slope-area plot or by applying Bayesian Optimization-based function (m/noptvar algorithm in TopoToolbox, see Schwanghart and Scherler 2014). Using the latter procedure, a best-fit θ of 0.40 was derived for the study area. Under certain conditions such as uniform lithology and climate, ksn can be considered as a proxy of uplift rates (Whipple and Tucker 1999; among others).

Chi analysis is the integral conversion of the slope-area plot, which is based on the use of a reference drainage area and a χ vs. elevation plot (Perron and Royden 2013):

$$\chi = \int_{xb}^{x} \left(\frac{A_0}{A(x)}\right)^{\frac{m}{n}} dx \tag{5}$$

where: A_0: reference drainage (usually 1 m^2); m/n or θ: concavity index (Perron and Royden 2013).

This method reduces topographic noise and can be useful for comparing the channel steepness in catchments of different sizes and/or along opposite sides. Combined with other metrics like channel gradients, local relief, and ksn, a χ map can represent one of the most effective topographic indices for the characterization of the dynamic stage and relative (un)stability of drainage divides (see for example Gioia et al. 2023). Here, we used the Tinitaly DEM, a reference concavity of 0.40, and sea-levels of the Tyrrhenian and Ionian Sea within the Topotoolbox-based TAK functions (Forte and Whipple 2018, 2019) for both the estimation of the χ map and assessment of drainage divide unstability.

A strong difference in χ values across the drainage divides on opposite sides delineated drainage divide sectors with a high geomorphic disequilibrium (*sensu* Forte and Whipple 2018). More specifically, aggressive channels show lower χ values, whereas victim patterns or captured channels exhibit higher values of χ (Willett et al. 2014; Gioia et al. 2023). Insights derived from the χ map were integrated by evaluating the values of other metrics such as relief, and channel gradient along opposite watersheds (Aristizábal and Korup 2025; Forte and Whipple 2018; Gioia et al. 2023). Such an approach allowed us to infer the arrangement of transient catchments, which have been compared to the spatial distribution of DLL landslides.

3.3 Statistical analysis

Statistical analysis of the relationships among the spatial distribution of landslides, lithological units, and landscape domains was performed to infer the main factors controlling the development and evolution of slope failures. Lithological and geomorphological conditioning factors were investigated using two detailed maps of the lithological and landscape features of the study area (Schiattarella et al. 2024). The influence of lithological features on landslide processes was investigated by estimating landslide area within each of the lithological classes of the geolithological map. The areal distribution of landslides was normalized by the outcrop areas of the different lithological classes to obtain a ratio independent of the area covered by each lithology. A value higher than 1 of this ratio furnished an estimation of the lithological classes where landslides occurred preferentially. The same approach was adopted for the comparison between landslide pattern and landscape units of the study area.

Proximity analysis between landslide polygons and drainage network was also estimated in a GIS environment to obtain a picture of the influence of fluvial processes on landslide occurrence. Such an analysis was complemented by investigating the spatial relationships among landslide polygons, higher values of ksn, and drainage divides of the transient catchments. Minimum vertical distance (i.e.: elevation difference) between the scar of each landslide (i.e. the highest point) and the nearest point of the transient divides was also estimated.

4 Results

4.1 Landslide distribution

Our landslide inventory includes about 14,200 landslides of different size and type (Fig. 4), which cover an area of about 720 km^2 and range in size from about 300 m^2 to 4.13×10^6 m^2. Approximately 8470 landslides were mapped within the IFFI project (black dots in Fig. 4). By considering the landslides mapped in the Protection Plan of the Basilicata river basin Authority mainly close to the urban areas (green dots in Fig. 4), we estimate a total landslide density of about 7.2%, with a non-random and highly-clusterized spatial distribution of the landslide phenomena. Although the landslides occurred across a wide range of elevation (i.e. from 5 to 1700 m a.s.l.) and slope (i.e.: from 2° to 80°), most of the phenomena are dis-

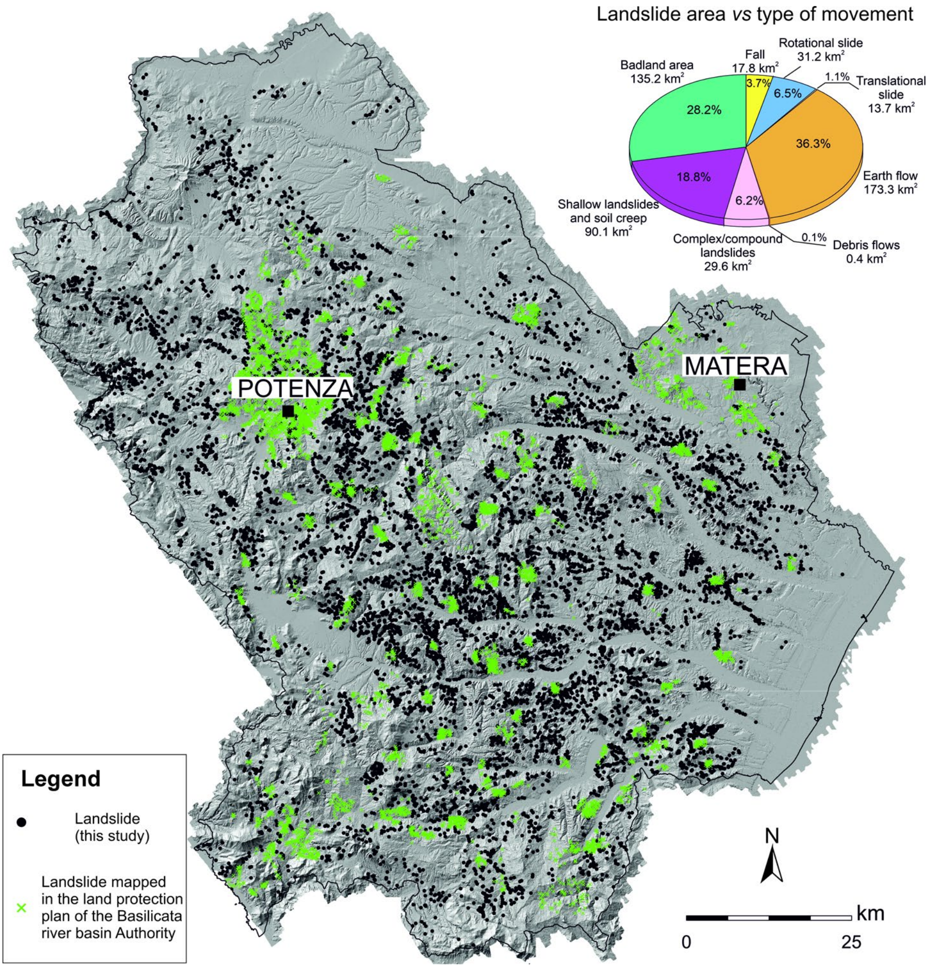

Fig. 4 LIM of the study area and basic statistics of the landslide types. Black (IFFI project) and green (land protection plan dataset) points mark the highest point of the landslides

tributed in a narrower altitude and slope bands: the interquartile ranges span mean altitude of 310–985 m a.s.l. and mean slopes of 9–30°.

Classification type of the landslides mapped in the IFFI project (Fig. 4) highlights that about 37% of the total landslide area has been classified as earthflows. Areas affected by shallow (i.e.: slip depth lower than 3 m) landslides cover an area of about 90 km^2, whereas rotational slides and complex movements developed on a surface of about 13 km^2. Rockfalls are prevalent along the steeper slopes of carbonate morphostructures, such as the rocky coasts of the inner zones and the fault slopes of the axial zone. The occurrence of these phenomena is driven by both high relief and degree of rock fracturation/tectonization (Minervino Amodio et al. 2024). Debris flows show a preferential distribution along the fault slopes (for example along the western fault slope of the Mt Alpi carbonate high) or at the outlet of steep valleys carved in Pliocene clastics.

Slow-moving landslides, rotational slides and deeper-seated phenomena mainly occurred in the axial and outer sectors of the belt, depicting local zones of high concentration of landslide processes. Such landslide-dominated landscapes can be recognized in several catchments of these sectors. They are typically affected by a complex superimposition of mass movements of different sizes, types, and ages. Smaller and shallower movements often represent the reactivations of larger and deep-seated landslides; a typical pattern is represented by complex/compound movements, with rotational slide in the headwater sectors that evolved in earthflow in their lower-altitude areas (Gioia et al. 2024a; Santangelo et al. 2013).

Landslide clustering does not appear to be controlled by rainfall distribution (for example cf. Figures 2 and 4), thus suggesting a prevalent geological and geomorphological control on the landslide pattern.

We mapped a dataset of about 470 larger, deeper and older landslides (DLL class). They are mainly concentrated in several catchments of the axial and outer zones of the belt, which are characterized by a complex litho-structural and tectonic setting, high landslide density, and widespread shallow movements.

4.2 Lithological and geomorphological control on the landslide pattern

Visual inspection of the relationships between landslide pattern and lithological units of the study area (Fig. 5) highlights that the clustering of the mapped landslides appears to be driven by the outcrops of specific lithological classes. The graph of the landslide area for each lithological class (Fig. 6) shows that 36% of the landslides occurred in Unit 17, which included chaotic and highly-deformed, varicoloured shale and clay with minor marly and calcareous components. Such a unit roughly corresponds to a geological formation, the Argille Varicolori group, which has been widely recognized as an important predisposing factor for landslide processes in the southern Apennine belt (see for example Borgomeo et al. 2014; Picarelli et al. 2005; Santangelo et al. 2013). Clusterization of the landslides in the axial and outer zones of the belt is also due to the preferential distribution of the landslide processes in the complex alternations of marls, clay and sandstone of Unit 16. As a matter of fact, about 13.6% of the landslides involved these bedrock deposits.

Approximately 193 km^2 of the landslide area (i.e.: 26.8% of the total landslide area) involved Lower Pleistocene marine clays of the foredeep, which are frequently affected by badlands and shallow movements. In the foredeep areas, about 6.5% of the slope failures also involved the coarser-grained foredeep deposits (Unit 11b in Figs. 5 and 6), which often represent the caprock of the foredeep landscape.

When we consider the ratio between landslide area and the areal extent of the lithological units (Fig. 6), a significant value of about 1.8 can be observed for Unit 17. Landslide frequency reaches a relevant value of about 2.2 in Unit 12, which groups Pliocene clastic deposits outcropping in the thrust-top basins of the mountain belt, while a value slightly higher than 1 of the normalization ratio can be estimated for Unit 16. Moreover, localized sectors of high susceptibility (values of the landslide normalized ratio higher than 1) can be observed where Unit 5 (i.e. volcanoclastic deposits of the Mt Vulture) outcrops. Such an analysis highlights that the presence of these lithological classes can be considered as an important predisposing factor for landslide occurrence in the study area.

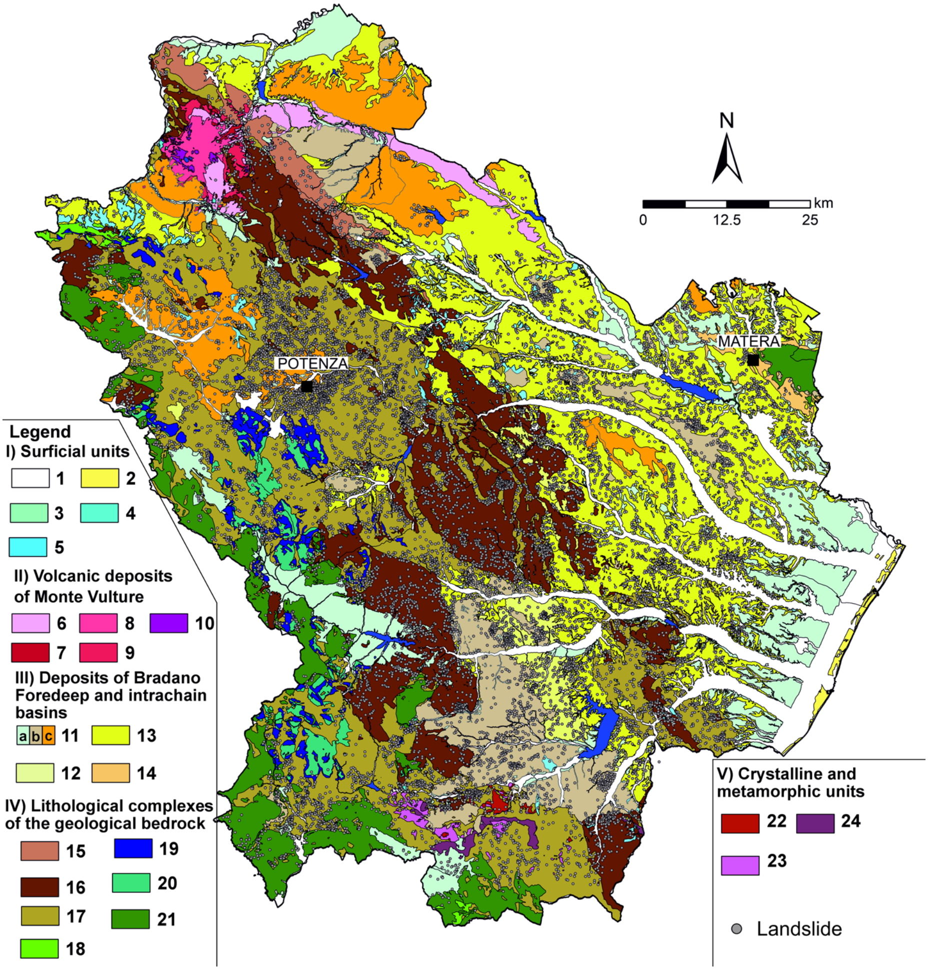

Fig. 5 Landslide pattern portrayed on the lithological map of the study area. Legend: 1: Loose deposits in active sedimentation (alluvial, colluvial, and slope deposits), 2: Loose or weakly-cemented sand (beach/dune system), 3: Terraced clastic deposits, 4: Travertine, 5: Matrix-supported or massive clay-sandy breccias (slope deposits); 6: Weakly cemented volcanoclastic conglomerates with sand, silt and primary volcanics, 7: Lava flows and domes, 8: Block tuffs with thin lava intercalations, 9: Lapilli tuff with volcanoclastic conglomerates, 10: Ash and lapilli with isolated lithic blocks, 11a) Clastic infill of Quaternary intermontane basins; 11b) foredeep and intrachain basin conglomerate and sand, hung on present-day thalwegs; 11c) sand and conglomerate constituting the hilly landscape of intrachain basins. 12: Sandstone with clay, 13: Blue-grey clay with lens-shaped weakly-cemented sandstones and conglomerates, 14: Calcarenite, 15: Limestone and marly limestone with clay and sandstone, 16: Sandstones and marly clays, 17: Varicoloured shale and clay with marly and calcareous component, in a chaotic setting and highly deformed beds, often broken and forming isolated blocks 18: Calcareous breccia and calcarenite, 19: Jasper, chert and radiolarites, 20: Limestone with chert beds and nodules, 21: Platform limestone and dolostone, 22: Tectonically fractured bodies of granite and gneiss, 23: Cataclastic serpentinites, metabasites and basalts, 24: Polydeformed metalimestones and shales

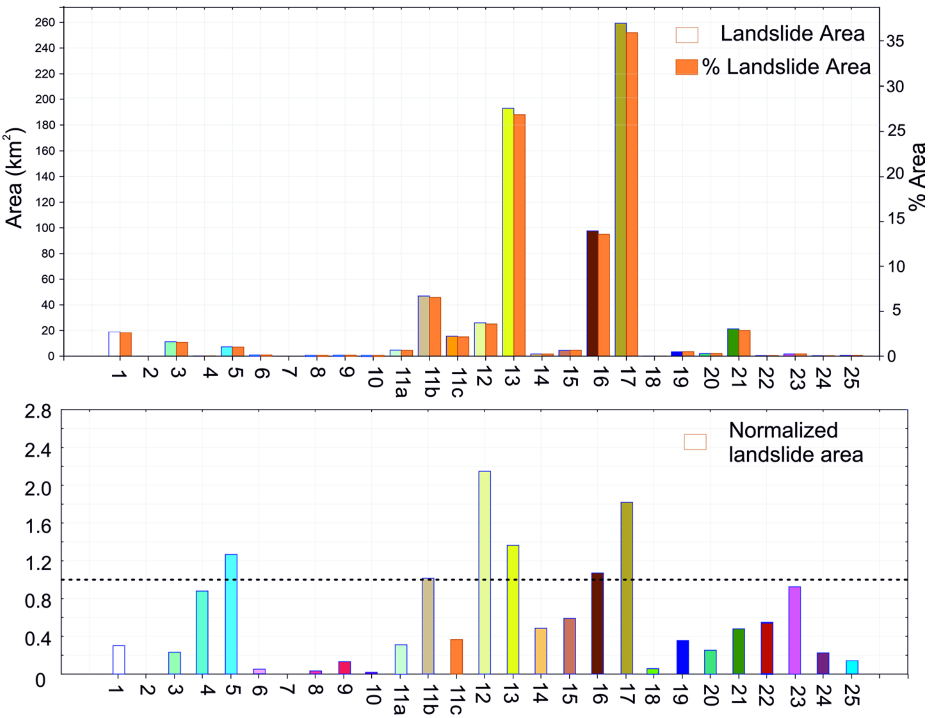

Fig. 6 Statistical relationships between lithological features and landslide occurrence. **Top:** Histogram showing the areal extent of landslides per each lithology (see Fig. 4 for details on the lithological classes); **Bottom:** histogram showing the frequency of landslides per unit area for each lithology. Values higher than 1 suggest a preferential occurrence of the landslides in the lithological class

We explore the possible influence of the landscape setting on the landslide pattern by comparing LIM with a detailed map of the landscape units of the study area (Fig. 7, see Schiattarella et al. 2024 for some more details on the approach and criteria of the map drawing). A preferential occurrence of landslides in the clayey landscape of the axial zone can be pointed out (Unit 8a in Fig. 8), with a landslide area of 174.7 km^2 and a percentage of the total area of about 25%.

Landslides tend to preferentially occur in the foredeep sectors, where the landslide area sums a value of approximately 245 km^2, corresponding to 34% of the total landslide area. The landslides are also widespread in Unit 5, which groups sandstone ridges and thrust sheets of the axial-outer zones of the mountain belt.

After the normalization based on the areal extent of the landscape units, a ratio of 1.6 can be attributed to the clayey landscape of the mountain belt. A factor slightly higher than 1 can be attributed to Unit 3, suggesting that this landscape unit can also be considered as a landslide-prone area.

In these sectors of the study area, landslides are widespread without a clear spatial connection with topographic factors such as mean relief, mean slope and integral hypsometric (Fig. 9). As a matter of fact, higher landslide density (i.e.: LD > 10%) occurred in catchments showing a high variability of these topographic parameters (Fig. 9), suggesting a potential role of tectonically-induced long-term landscape evolution on the landslide pattern. In par-

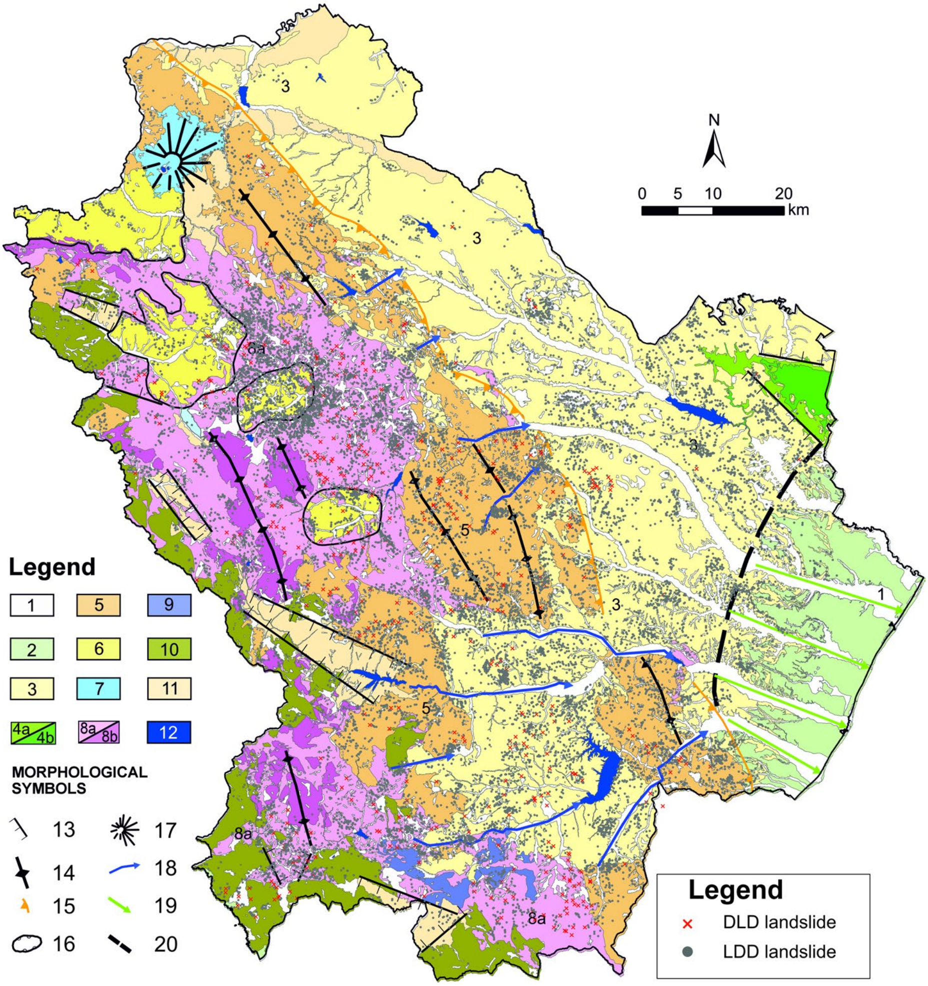

Fig. 7 Landscape units of the study area and landslide distribution. The map also shows the distribution of the DLD and LDD class. Note the preferential distribution of the DLD landslides along the clayey landscape of the axial and the monoclinal ridges of the outer zones. Legend: (1) River plains and recent surficial deposits (alluvial, slope, and colluvial deposits); (2) Coastal plains and marine terraces (3) Bradano Foredeep and Sant'Arcangelo basin; (4) Murgia of Matera (foreland morpho-structural high) with epigenetic gorges: (a) Gravina Calcarenites (Pleistocene); (b) Altamura Limestone (Upper Cretaceous); 5) Sandstone ridges of the external zone of the chain; 6) Pliocene-Pleistocene intrachain basins; 7) Mount Vulture Volcano; 8) Axial mountain ranges: (a) clayey landscape; (b) calcareous-siliceous ridges; 9) Ophiolite-bearing shaly hills; 10) Carbonate ridges; 11) Quaternary intermontane basins; 12) Artificial lakes; 13) Limit of the intermontane basins and/or morpho-structural highs (the dashes indicate the downthrowing blocks); 14) Morphological axis of a mountain ridge; 15) "External" (eastern) morphological front of the chain; 16) Pliocene intrachain basin area; 17) Volcano; 18) Discordant drainage; 19) Parallel pattern rivers; 20) Inner limit of the marine terraced area

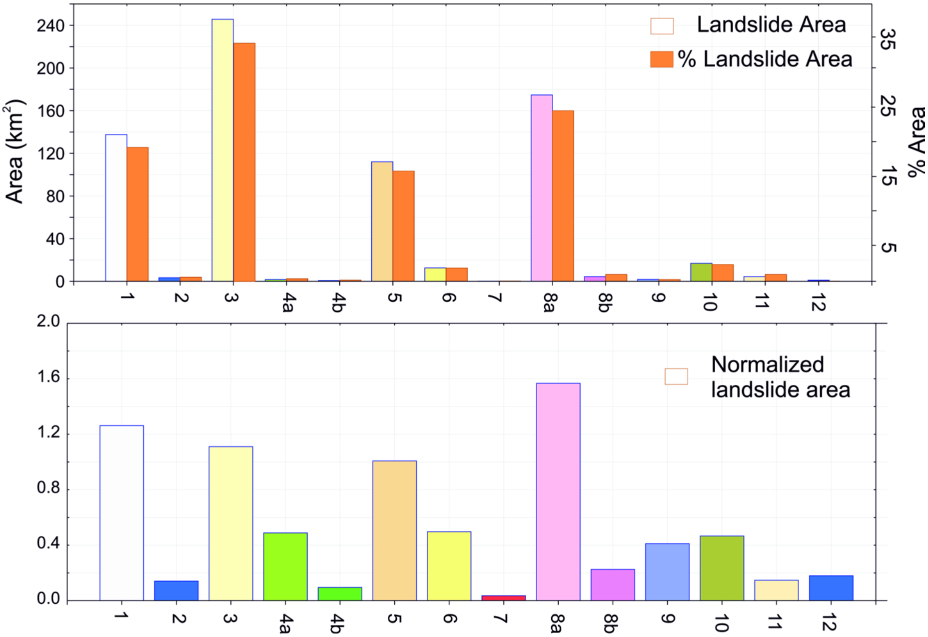

Fig. 8 **Top:** Histogram showing the frequency distribution of landslide area for each landscape unit (numbering of the landscape units is the same of Fig. 6); **Bottom:** histogram showing the frequency of landslides per unit area for each landscape unit

ticular, DLL landslides exhibit peculiar features: they are concentrated in the axial and outer zones of the chain (Fig. 7), and their scarps show an articulated shape. Another key feature is that they are often located near watersheds of high-order catchments.

4.3 Landslide distribution and landscape metrics

The potential influence of fluvial incision on the landslide pattern was investigated by estimating the proximity relationship between mapped landslides and fluvial networks. The analysis highlights that approximately 70% of the channels interact with the mapped landslides and 87% of them have a channel at a distance lower than 50 m.

Landscape metrics derived from the stream power model can be used to predict the degree of tectonic perturbation and geomorphologic disequilibrium of a tectonically-controlled landscape, providing additional information on the role of the fluvial incision in the development and evolution of mass movement phenomena in the study area.

Ksn values are strongly controlled by lithological features, although a systematic increase of the mean and std values of the index can be observed for the channels that interact with the mapped landslides (see box plots in Fig. 10). Visual inspection of the ksn map and basic statistics (mean and std of the ksn higher in the landslide area, see frame in Fig. 10) revealed a preferential location of landslides in areas featured by higher ksn values. For example, a significant increase from 12 to 16.3 of the mean ksn values was estimated for the channels that interacted with the landslides. Such a trend was systematically recognized for all the

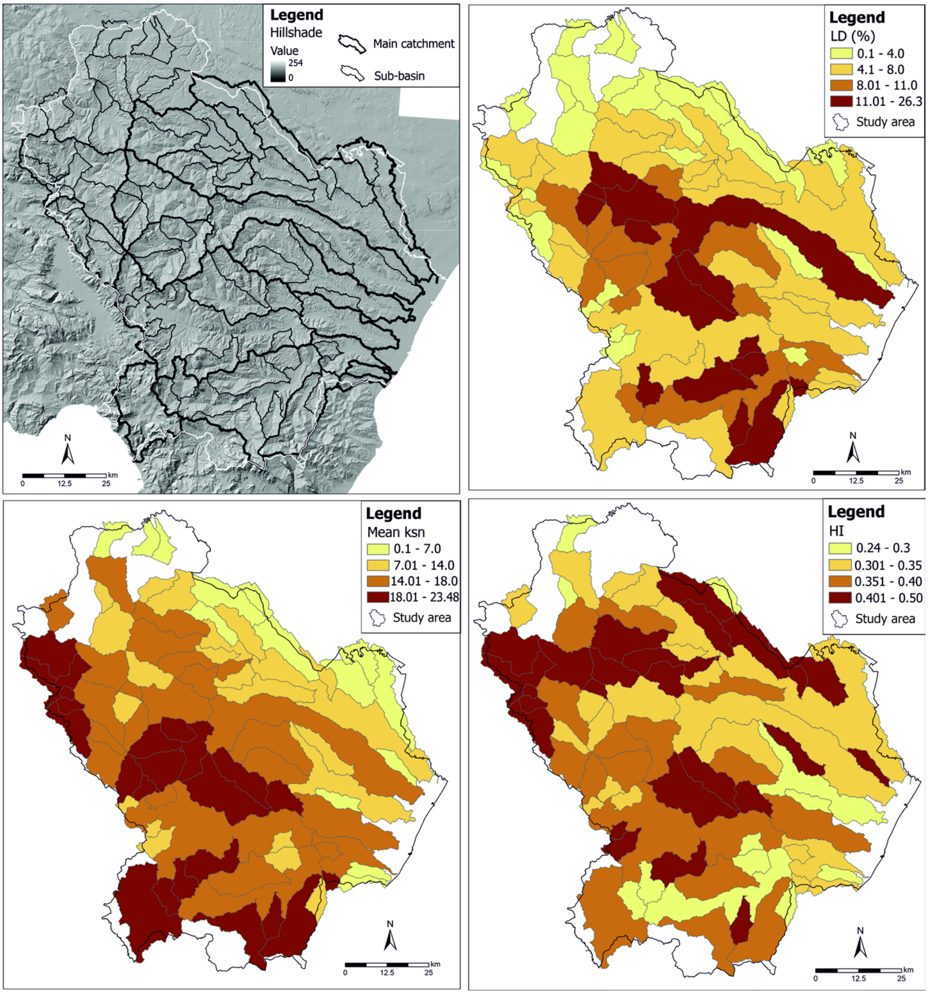

Fig. 9 Catchment-based distribution of the mean values of landslide density (LD), ksn (normalized channel steepness index), and hypsometric integral (HI)

lithological classes and landscape units with a preferential occurrence of the landslides (i.e.: units with a value of the ratio higher than 1, Figs. 6 and 8).

Therefore, analysis of the spatial relationships between mapped landslides and drainage networks suggests a strong influence of tectonic-induced fluvial incision in promoting mass movement processes. More specifically, under similar lithological and climate conditions, higher ksn values should indicate local increase in surface uplift, which in turn can cause disequilibrium and thus landsliding.

The spatial distribution of the mapped landslides differs markedly between DLD and LDD class: the latter tend to cluster near to drainage divides, which likely represent sectors of the landscape featured by a high degree of geomorphological disequilibrium in the long-term evolutionary history of the study area. The χ map has been largely used as a proxy of the degree of dis(equilibrium) of opposite drainage and, more in general, for the identifica-

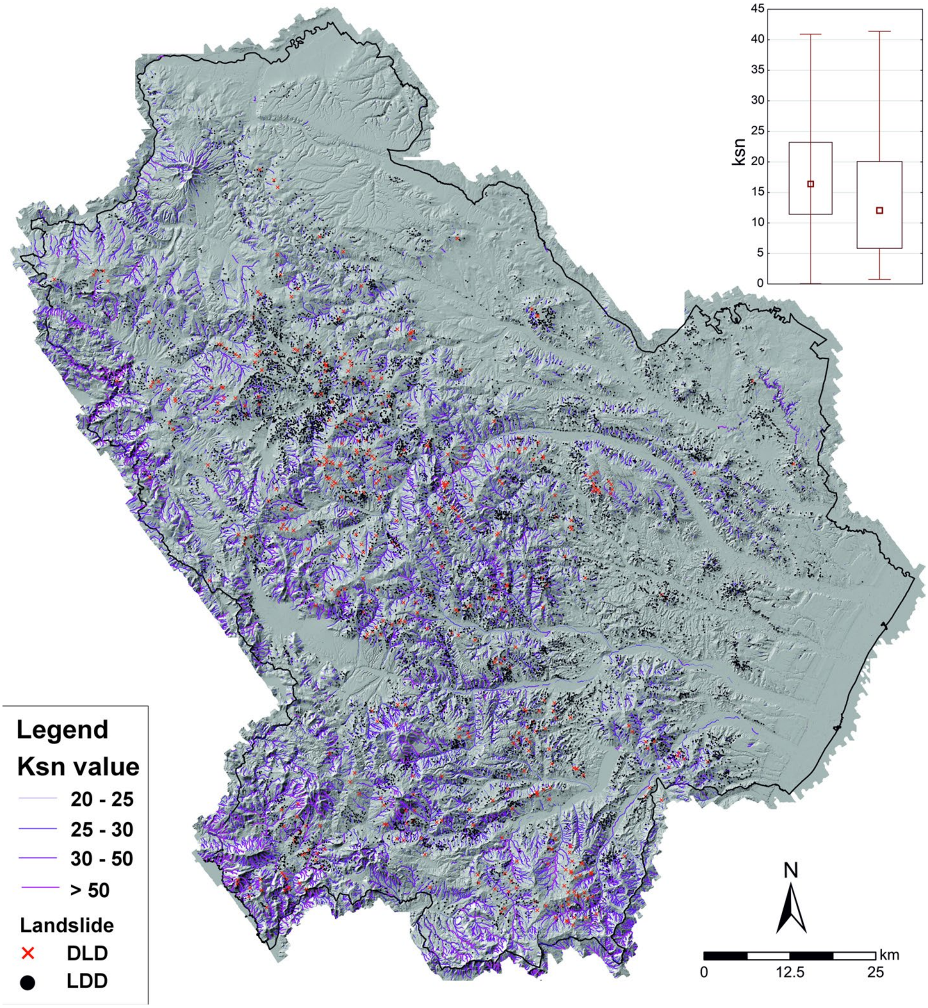

Fig. 10 Spatial distribution of ksn and its relationships with the DLD and LDD landslide classes. In the frame: box plots showing the relationships between ksn values and landslide pattern. Left: channels that interact with landslides; right: non-overlapping between channels and landslides

tion of the transient catchments. High differences in the χ values along the opposite drainage divides have been used to delineate unstable or transient catchments (Fig. 11). The map highlights pronounced contrasts in χ values along a N-S trending strip that separated main catchments of the Ionian side from the Tyrrhenian ones. Such a strong contrast clearly marks the aggressor pattern of the tributaries of the main rivers flowing toward the Tyrrhenian Sea (i.e. the Noce and Sele rivers). We can also detect a marked difference in χ values and a western direction of the inferred migration in several catchments of the axial zone draining toward the Ionian Sea.

We detect that most of the larger landslides of the study area are located near unstable drainage divides. As a matter of fact, the frequency distribution of the minimum distance

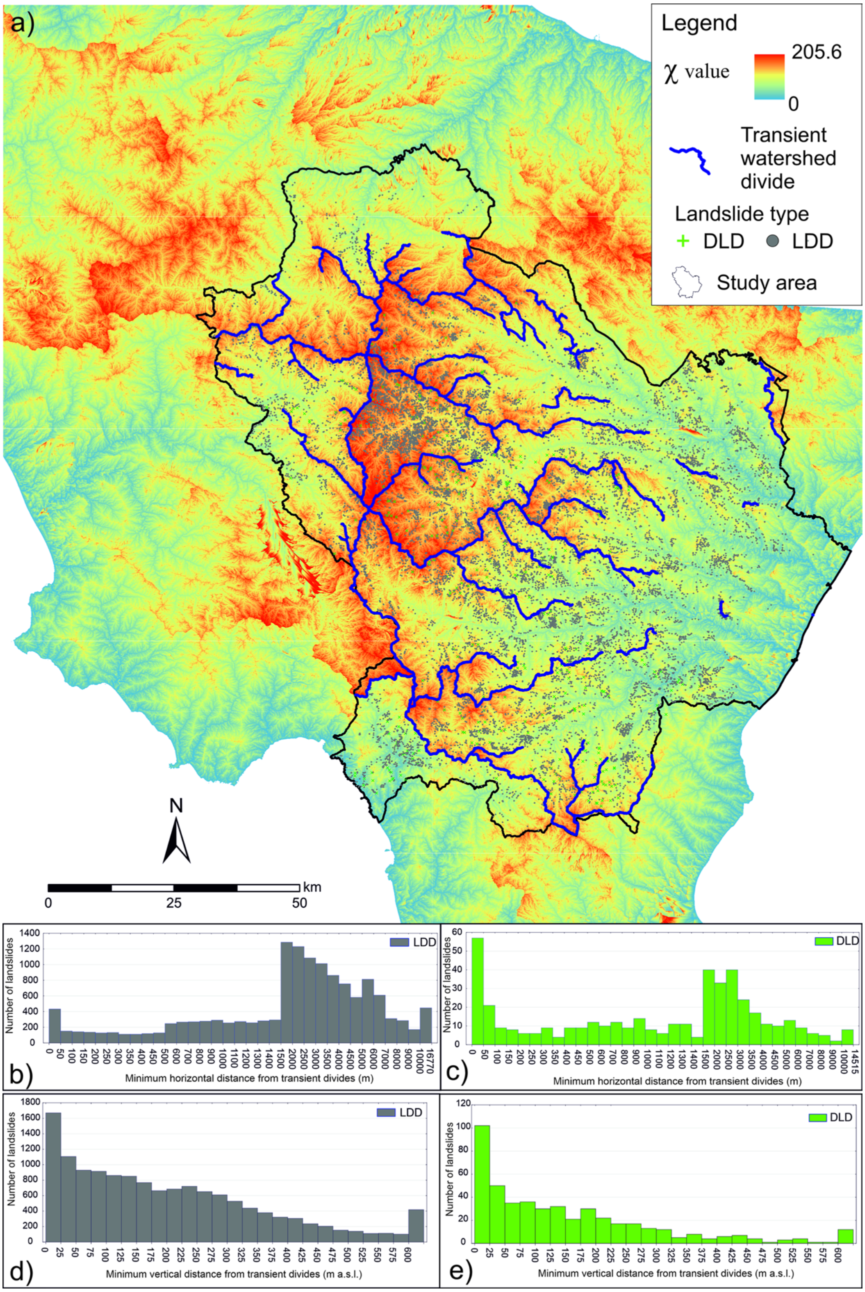

Fig. 11 **a** Distribution of χ values along the drainage network of the study area, transient divides and their relationships with DLD and LDD landslides. Histograms show the minimum horizontal and vertical distance of the landslides from the nearest transient divide. **b** minimum distance between DLD landslides and the nearest transient divide; **c** minimum distance between LDD and the nearest transient divide; **d** vertical distance (i.e.: elevation difference) between the highest point of the DLD landslides and the nearest transient divide; **e** vertical distance between LDD class and the nearest transient divide;

between DLL landslides and transient divides shows a peak (i.e. about 15% of the total DLL landslides) for a distance lower than 50 m (Fig. 11c). A similar strict relationship can be inferred from the vertical distance (i.e.: height difference between highest point of a landslide and the nearest transient divide) between landslides and transient divides. Indeed, approximately 30% of the DLLs are located at a vertical distance lower than 50 m a.s.l. to the nearest transient catchment. Such quantitative analyses and independent geomorphic evidence of accelerated river incision suggest a relevant role of transient catchments in the occurrence of deep-seated landslides during long-term stages of landscape evolution and river incision. Indeed, these mass movements represent the most impressive slope failures of the study area (see for example Fig. 3).

5 Discussion

Litho-structural setting and geomorphological features of the southern Apennines are the result of a complex morphotectonic evolution, which promoted Quaternary relief growth, pronounced fluvial incision and widespread slope processes. Landslide density of the study area is slightly higher than 7% and the spatial distribution of the landslide phenomena in such a Mediterranean climate is featured by well-recognizable clusters or zones of high landslide susceptibility, which can be attributed to the influence of geological and geomorphological driving factors. Slow-moving and shallow landslides are the most abundant slope failure phenomena, although landslide-dominated landscapes or local zones of higher landslide density are featured by the coexistence of complex, deep-seated and large mass movements and shallower/smaller ones.

Statistical analysis of the LIM revealed that lithology exerts a primary control on landslide pattern, with a preferential distribution in outcrop areas of chaotic shaly rocks (i.e. the different tectono-stratigraphic units included in the Argille Varicolori group). As a matter of fact, landslide occurrence in this lithological class is about 2 times higher than other units. Such a high susceptibility of this scaly clay is well-documented (Borgomeo et al. 2014; Santangelo et al. 2013) and was related to the complex and highly-tectonized chaotic structure of the shaly rock, which favoured a strong and rapid decrease of the material strength in response to the increase of water content (Picarelli et al. 2005). Our analysis also showed that recent loose deposits and Pliocene clastics are sectors of preferential distribution of landslide processes. Lithological control on the landslide clustering in the axial and outer zone of the belt is also due to the preferential distribution of the landslide processes in both the Pliocene clastic deposits and structurally- and stratigraphically-complex bedrock units of the chain front.

Landslide processes also tend to preferentially develop in some landscape units of the study area, such as the clayey landscape of the mountain belt and the monoclinal ridges of the chain front. Widespread landslide phenomena in several sectors of the axial and frontal sectors of the southern Apennines have been generally ascribed to different predisposing factors such as litho-structural and tectonic setting, relief growth and poor geotechnical properties of these rocks (Ardizzone et al. 2023; Borgomeo et al. 2014; Cendrero and Dramis 1996; Conforti et al. 2013; Gioia et al. 2024a; Picarelli et al. 2005; Santangelo et al. 2014), but comprehensive investigations at a regional scale are lacking.

Deeper analysis of the relationships between landslide density and landscape features highlights that the preferential occurrence of the landslides in these morphotectonic domains can be only partially ascribed to the lithological features or topographic features of this landscape unit. For example, we observe a high variability of the landslide density in different catchments carved in Argille Varicolori complex or clay-rich deposits of the axial zone. We also observe a high variability of mean topographic parameters in catchments with a large difference in landslide density (mean slope and relief in Fig. 12).

This high variability and the absence of correlation appear more evident when we consider only the catchments of the axial and outer zones of the belt. We can explore the potential role of the tectonically-driven fluvial incision on the landslide distribution by analyzing the drainage network and topographic metrics related to the stream power model. Spatial relations of distance from streams and landslides suggest the direct control of the fluvial net on the initiation and evolution of slope failure processes. In addition, metrics of the degree of transience and geomorphologic disequilibrium at a catchment scale, such as HI and ksn indexes (Fig. 12) show a correlation with the increase of LD. In fact, our analysis infers an inverse correlation between hypsometric integral and landslide density, while a positive correlation can be observed between LD and mean ksn.

Quaternary uplift of the chain was generally ascribed to the thermal/isostatic raising of the chain coupled with fault activity (Schiattarella et al. 2003). Extensional tectonics and local faulting of the axial zone are well recognized, while the possible recent (i.e. late

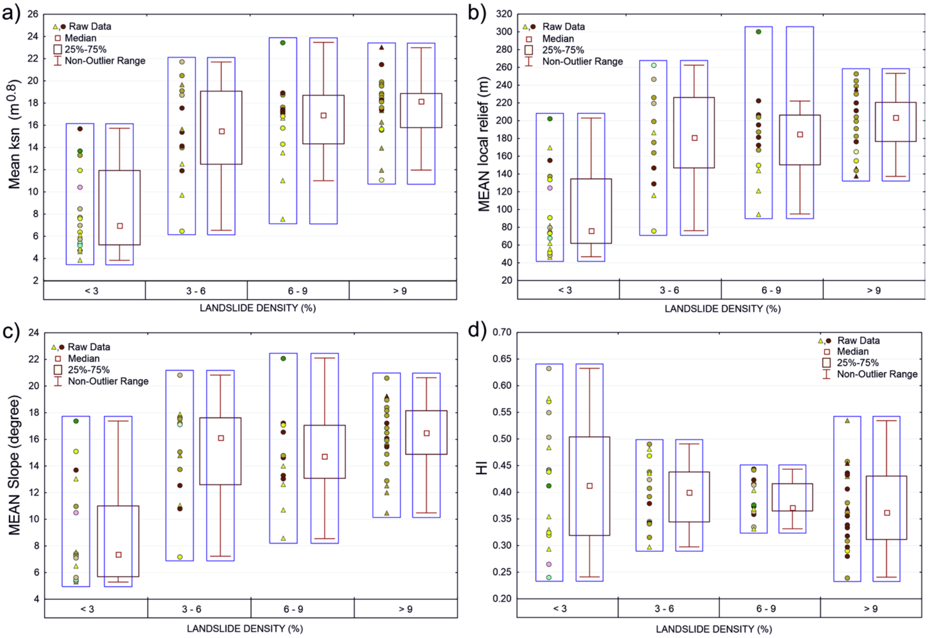

Fig. 12 Variability and box plots of mean values of ksn (**a**), relief (**b**), slope (**c**), and hypsometric integral (**d**) for the catchments of the study area (see Fig. 8 for the catchment location), grouped on the basis of four different classes of landslide density (<3%, 3–6%, 6–9%, >9). Raw data of the variability plots are coloured according to the main lithological class of the catchment (same colour scheme used in Fig. 6); a triangle shows catchments with the prevalence of a single lithological class (outcrop area>70%), whereas a circle indicates outcrops of two or more lithological classes

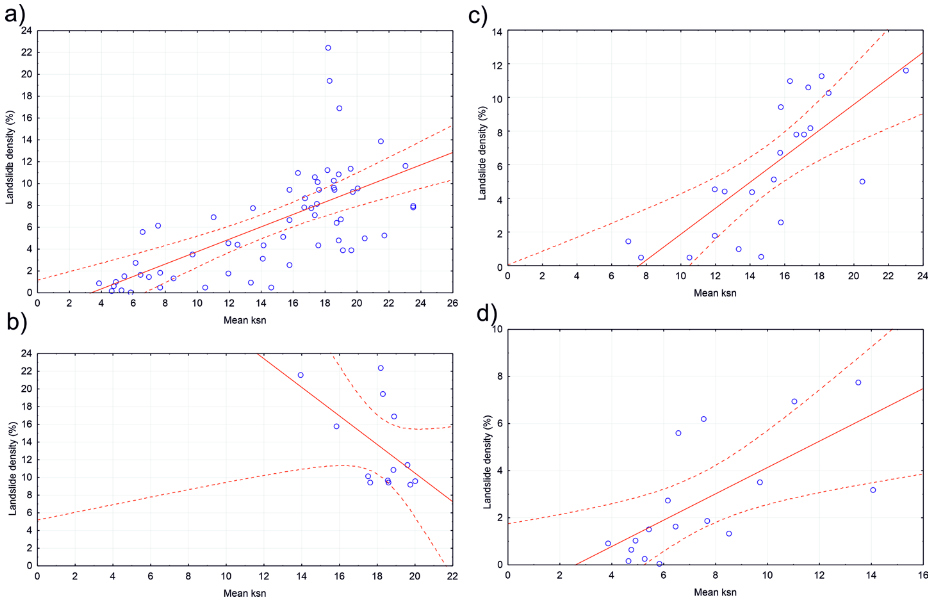

Fig. 13 Catchment-averaged scatterplots of the landslide density (LD) against mean ksn values. **a** entire area; **b** axial zone; **c** outer zone; **d** foredeep. Red lines indicate the best fit of linear regression, whereas dashed ones represent 98% confidence intervals. Regression coefficients are: 0.33 (**a**); 0.29 (**b**); 0.57 (**c**); 0.47 (**d**)

Quaternary) activity of blind thrust is more debated. In addition, few data are available for a regional estimation of the uplift rates but a high spatial and temporal variability of the uplift rates of the study area can be inferred from previous data. Thus, our morphometric analyses can provide an estimation of the uplift rate distribution and/or the transient state of the landscape. Under certain conditions and assumptions (i.e. similar lithological features), ksn can be considered a proxy of the uplift rates. A positive correlation between ksn and LD (Fig. 13) for several catchments of the clayey axial zone can be estimated. Such a relation can support the idea of a link between landslide occurrence and irregular spatial distribution of surface uplift.

Moreover, we observe that larger and deeper landslides of the study area are preferentially distributed in transient catchments and close to main drainage divides, suggesting the occurrence of larger and older landslides during stages of a high degree of geomorphologic disequilibrium of the fluvial system. In the absence of robust chronological constraints on the initiation of such landslide processes, we can only hypothesize the morphotectonic setting that can favour the occurrence of these phenomena. The drainage evolution of the study area is strongly featured by a dramatic base-level fall during the Middle Pleistocene, which coincided with the post-lacustrine phase of the main tectonic depressions (Giano et al. 2014; Gioia et al. 2023; Schiattarella et al. 2003, 2017). It is likely that the main and larger landslide phenomena occurred in response to the aggressor pattern of migrating drainage nets driven by fast base-level falls. Alternatively, significant changes in slope hydrology driven by Late Quaternary climate oscillations should be considered as a possible triggering factor for the activation of large, deep-seated landslides during morphotectonic stages characterized by high geomorphological disequilibrium (see for example Borgatti and Soldati 2010; Gioia et al. 2011; Pánek 2014).

6 Concluding remarks

The analysis of a detailed geomorphological landslide inventory of a large sector of the southern Apennines, Italy was carried out in order to investigate the relationships between geological and geomorphological factors and landslide distribution. Statistical analyses and comparison between landslide pattern, thematic (i.e. lithological and landscape units) maps and morphometric parameters of the landscape dynamics allowed us to infer the main predisposing factors of the landslide pattern and infer a relevant role of fluvial incision and catchment disequilibrium in the landslide occurrence.

Our results highlighted a total landslide density of the study area of about 7%, a primary control of the lithological features on the landslide distribution and localized sectors of landslide clustering. Slow-moving and shallow landslides are the prevalent landslide type; they mainly develop in the axial and outer domains of the chain and involved chaotic shaly rocks, Pliocene clastics or highly-tectonized alternations of marls, clay and sandstone. Landslide-dominated landscapes and catchments with higher landslide density often exhibit a complex superimposition of polyphasic and diachronous mass movements. Analysis of the relationships between landslide pattern and metrics of landscape evolution suggests a significant role of tectonically-induced landscape disequilibrium, with landslide processes that tend to occur in transient catchments or experiencing uplift and fluvial incision. On the other hand, larger, older and deep-seated landslides are preferentially preserved close to transient divides. Such evidence as well as the inverse correlation between hypsometric integral and landslide density support the idea of an activation of these phenomena during past phases of drainage network evolution and disequilibrium.

Acknowledgements We gratefully acknowledge the support of the guest editors as well as the two anonymous reviewers for detailed comments and constructive criticism, which helped to improve this paper. This paper greatly benefited from the discussion within the Working Group of 'SIStemi e TECnologie integrati per l'analisi morfoTettonica'(SISTECT) of the AIGeo(Associazione Italiana di Geografia Fisica e Gemorfologia).

Author contributions Dario Gioia ideated the study conception and design. Material preparation, data collection and analysis were performed by Dario Gioia with the support of Giuseppe Corrado, Antonio Minervino Amodio, Lucia Contillo and Marcello Schiattarella. The first draft of the manuscript was written by Dario Gioia and all authors commented on previous versions of the manuscript. All authors read and approved the final manuscript.

Funding Open access funding provided by Consiglio Nazionale Delle Ricerche (CNR) within the CRUI-CARE Agreement. The authors declare that no funds, grants, or other support were received during the preparation of this manuscript.

Declarations

Conflict of interest The authors have no relevant financial or non-financial interests to disclose.

References

Ardizzone F, Bucci F, Cardinali M, Fiorucci F, Pisano L, Santangelo M, Zumpano V (2023) Geomorphological landslide inventory map of the Daunia Apennines, Southern Italy. Earth Syst Sci Data 15(2):753–767. https://doi.org/10.5194/essd-15-753-2023

Aristizábal E, Korup O (2025) Linking landslide patterns to transient landscapes in the Northern Colombian Andes. J Geophys Research: Earth Surf. https://doi.org/10.1029/2024jf008027

Ascione A, Ciarcia S, Di Donato V, Mazzoli S, Vitale S (2012) The Pliocene-Quaternary wedge-top basins of southern Italy: an expression of propagating lateral slab tear beneath the Apennines. Basin Res 24(4):456–474. https://doi.org/10.1111/j.1365-2117.2011.00534.x

Ascione A, Mazzoli S, Petrosino P, Valente E (2013) A decoupled kinematic model for active normal faults: insights from the 1980, ms = 6.9 irpinia earthquake, Southern Italy. Bull Geol Soc Am 125(7–8):1239–1259. https://doi.org/10.1130/B30814.1

Bentivenga M, Giocoli A, Palladino G, Perrone A, Piscitelli S (2019) Geological and geophysical characterization of the Brindisi di Montagna Scalo landslide (Basilicata, Southern Italy). Geomatics Nat Hazards Risk 10(1):1367–1388. https://doi.org/10.1080/19475705.2019.1575291

Bentivenga M, Prosser G, Guglielmi P, Palladino G, Piccarreta M, Straziuso K, Cavalcante F (2023) Landslides and predisposing factors of the Southern Apennines, Italy. J Maps. https://doi.org/10.1080/17445647.2022.2137065

Bentivenga M, Palladino G, Bellanova J, Calamita G, Perrone A, Piscitelli S, Rizzo E, Pepe A, Falabella F (2026) An interdisciplinary study of the Pietra Maura earthflow in the Marsico Nuovo territory (Southern Italy). Landslides 23(3):823–836. https://doi.org/10.1007/s10346-025-02667-9

Bian M, Qiu H, Chen X (2025) The distribution characteristics of large landslides along the Daduhe River in the Eastern Tibetan Plateau and their effects on landscape evolution. Remote Sens. https://doi.org/10.3390/rs17071133

Borgatti L, Soldati M (2010) Landslides as a geomorphological proxy for climate change: a record from the Dolomites (Northern Italy). Geomorphology 120(1):56–64. https://doi.org/10.1016/j.geomorph.2009.09.015

Borgomeo E, Hebditch KV, Whittaker AC, Lonergan L (2014) Characterising the spatial distribution, frequency and geomorphic controls on landslide occurrence. Molise Italy Geomorphology 226:148–161. https://doi.org/10.1016/j.geomorph.2014.08.004

Bucci F, Santangelo M, Fiorucci F, Ardizzone F, Giordan D, Cignetti M, Notti D, Allasia P, Godone D, Lagomarsino D, Pozzoli A, Norelli E, Cardinali M (2021) Geomorphologic landslide inventory by air photo interpretation of the High Agri Valley (Southern Italy). J Maps 17(2):376–388. https://doi.org/10.1080/17445647.2021.1943552

Calcaterra S, Cesi C, Di Maio C, Gambino P, Merli K, Vallario M, Vassallo R (2012) Surface displacements of two landslides evaluated by GPS and inclinometer systems: a case study in Southern Apennines, Italy. Nat Hazards 61(1):257–266. https://doi.org/10.1007/s11069-010-9633-3

Cendrero A, Dramis F (1996) The contribution of landslides to landscape evolution in Europe. Geomorphology 15:3–4.

Cocco M, Selvaggi G, Di Bona M, Basili A (1993) Recent seismic activity and earthquake occurrence along the Apennines. In Boschi E, Mantovani E, and Morelli A (eds.) Recent evolution and seismicity of the mediterranean region, Springer Netherlands, pp. 295–312. https://doi.org/10.1007/978-94-011-2016-6_15

Conforti M, Pascale S, Pepe M, Sdao F, Sole A (2013) Denudation processes and landforms map of the Camastra River catchment (Basilicata - South Italy). J Maps 9(3):444–455

Conforti M, Pascale S, Sdao F (2015) Mass movements inventory map of the Rubbio stream catchment (Basilicata – South Italy). J Maps 11(3):454–463. https://doi.org/10.1080/17445647.2014.924038

Conforti M, Mercuri M, Borrelli L (2021) Morphological changes detection of a large earthflow using archived images, lidar-derived dtm, and uav-based remote sensing. Remote Sens 13(1):1–25. https://doi.org/10.3390/rs13010120

Corrado G, Amodio S, Aucelli PPC, Gioia D, Pappone G, Schiattarella M (2025) Reconstructing active tectonics from land–sea correlations based on cross-interpretation of core and seismic data for the Tyrrhenian coastal segment in southern Italy. Earth Surf Proc Land 50(1);e6049. https://doi.org/10.1002/esp.6049

Cruden DM, Varnes DJ (1996) Landslide types and processes. In: Turner AK, Shuster RL (eds) Landslides: investigation and mitigation, National Academies, Washington DC, pp 36–75

Delchiaro M, Della Seta M, Martino S, Nozaem R, Moumeni M (2023) Tectonic deformation and landscape evolution inducing mass rock creep driven landslides: the Loumar case-study (Zagros Fold and Thrust Belt, Iran). Tectonophysics 846:229655. https://doi.org/10.1016/j.tecto.2022.229655

Di Maio C, Fornaro G, Gioia D, Reale D, Schiattarella M, Vassallo R (2018) In situ and satellite long-term monitoring of the Latronico landslide, Italy: displacement evolution, damage to buildings, and effectiveness of remedial works. Eng Geol 245:218–235. https://doi.org/10.1016/j.enggeo.2018.08.017

Discenza ME, Esposito C, Di Luzio E, Delchiaro M, Di Martire D, Minnillo M, Rouhi J, Martino S, Della Seta M, Troiani F, Calcaterra D, Mugnozza GS (2023) Deep-seated gravitational slope deformations in Molise region (Italy): novel inventory and main geomorphological features. J Maps. https://doi.org/10.1080/17445647.2022.2163198

Forte AM, Whipple KX (2018) Criteria and tools for determining drainage divide stability. Earth Planet Sci Lett 493:102–117. https://doi.org/10.1016/j.epsl.2018.04.026

Forte AM, Whipple KX (2019) Short communication: the topographic analysis kit (TAK) for TopoToolbox. Earth Surf Dynam 7(1):87–95. https://doi.org/10.5194/esurf-7-87-2019

Gallen SF, Wegmann KW, Frankel KL, Hughes S, Lewis RQ, Lyons N, Paris P, Ross K, Bauer JB, Witt AC (2011) Hillslope response to knickpoint migration in the Southern Appalachians: implications for the evolution of post-orogenic landscapes. Earth Surf Proc Land 36(9):1254–1267. https://doi.org/10.1002/esp.2150

Giano SI, Gioia D, Schiattarella M (2014) Morphotectonic evolution of connected intermontane basins from the southern Apennines, Italy: the legacy of the pre-existing structurally controlled landscape. Rend Lincei 25:241–252. https://doi.org/10.1007/s12210-014-0325-x

Gioia D, Leo P, Giano SI, Schiattarella M (2011) Chronological constraints on a holocene landslide in an intermontane basin of the southern Apennines, Italy: morphological evolution and palaeoclimate implications . Holocene 21(2):263–273. https://doi.org/10.1177/0959683610378879

Gioia D, Corrado G, Danese M, Minervino Amodio A, Schiattarella M (2023) Post-lacustrine evolution of a tectonically-controlled intermontane basin: drainage network analysis of the Mercure basin, Southern Italy. Front Earth Sci 11:1112067. https://doi.org/10.3389/feart.2023.1112067

Gioia D, Corrado G, Minervino Amodio A, Schiattarella M (2024a) Multi-temporal morphological analysis coupled to seismic survey of a mass movement from southern Italy: a combined tool to unravel the history of complex slow-moving landslides. Nat Hazards 120(14):13407–13432. https://doi.org/10.1007/s11069-024-06751-6

Gioia D, Corrado G, Amodio M, A., Schiattarella M (2024b) Uplift rate calculation based on the comparison between marine terrace data and river profile analysis: a morphotectonic insight from the Ionian coastal belt of Basilicata, Italy. Geomorphology 447:109030. https://doi.org/10.1016/j.geomorph.2023.109030

Guzzetti F, Mondini AC, Cardinali M, Fiorucci F, Santangelo M, Chang KT (2012) Landslide inventory maps: new tools for an old problem. Earth Sci Rev 112(1–2):42–66

Hungr O, Leroueil S, Picarelli L (2014) The Varnes classification of landslide types, an update [Review]. Landslides 11(2):167–194. https://doi.org/10.1007/s10346-013-0436-y

Kashyap A, Behera MD (2023) Geomorphic response of bedrock landslides induced landscape evolution across the Teesta catchment, Eastern Himalaya. Environ Earth Sci. https://doi.org/10.1007/s12665-023-10859-6

Korup O, Densmore AL, Schlunegger F (2010) The role of landslides in mountain range evolution. Geomorphology 120(1–2):77–90. https://doi.org/10.1016/j.geomorph.2009.09.017

Lague D (2014).The stream power river incision model: evidence, theory and beyond. Earth Surf Process Landf 39(1):38–61. https://doi.org/10.1002/esp.3462

Lazzari M, Gioia D (2016) Regional-scale landslide inventory, central-western sector of the Basilicata region (Southern Apennines, Italy). J Maps 12(5):852–859. https://doi.org/10.1080/17445647.2015.1091749

Lazzari M, Gioia D, Anzidei B (2018) Landslide inventory of the Basilicata region (Southern Italy). J Maps 14(2):348–356. https://doi.org/10.1080/17445647.2018.1475309

Lindsay JB (2016) Whitebox GAT: a case study in geomorphometric analysis. Comput Geosci 95:75–84. https://doi.org/10.1016/j.cageo.2016.07.003

Liu F, Li J, Yang S (2015) Landslide erosion associated with the Wenchuan earthquake in the Minjiang River watershed: implication for landscape evolution of the Longmen Shan, eastern Tibetan Plateau [Article]. Nat Hazards 76(3):1911–1926. https://doi.org/10.1007/s11069-014-1575-8

Menardi Noguera A, Rea G (2000) Deep structure of the Campanian-Lucanian Arc (Southern Apennine, Italy). Tectonophysics 324:239–265

Minervino Amodio A, Corrado G, Gallo IG, Gioia D, Schiattarella M, Vitale V, Robustelli G (2024) Three-dimensional rockslide analysis using unmanned aerial vehicle and LiDAR: the castrocucco case study, Southern Italy. Remote Sens. https://doi.org/10.3390/rs16122235

Ouimet WB, Whipple KX, Royden LH, Sun Z, Chen Z (2007) The influence of large landslides on river incision in a transient landscape: eastern margin of the Tibetan Plateau (Sichuan, China). Bull Geol Soc Am 119(11–12):1462–1476. https://doi.org/10.1130/B26136.1

Pánek T (2014) Recent progress in landslide dating. Progress Phys Geography: Earth Environ 39(2):168–198. https://doi.org/10.1177/0309133314550671

Perron JT, Royden L (2013) An integral approach to bedrock river profile analysis. Earth Surf Proc Land 38(6):570–576. https://doi.org/10.1002/esp.3302

Perrone A, Canora F, Calamita G, Bellanova J, Serlenga V, Panebianco S, Tragni N, Piscitelli S, Vignola L, Doglioni A, Simeone V, Sdao F, Lapenna V (2021) A multidisciplinary approach for landslide residual risk assessment: the Pomarico landslide (Basilicata Region, Southern Italy) case study. Landslides 18(1):353–365. https://doi.org/10.1007/s10346-020-01526-z

Pescatore T, Renda P, Schiattarella M, Tramutoli M (1999) Stratigraphic and structural relationships between Meso-Cenozoic Lagonegro basin and coeval carbonate platforms in Southern Apennines. Italy Tectonophysics 315(1–4):269–286. https://doi.org/10.1016/S0040-1951(99)00278-4

Picarelli L, Urciuoli G, Ramondini M, Comegna L (2005) Main features of mudslides in tectonised highly fissured clay shales. Landslides 2(1):15–30. https://doi.org/10.1007/s10346-004-0040-2

Roering JJ, Mackey BH, Handwerger AL, Booth AM, Schmidt DA, Bennett GL, Cerovski-Darriau C (2015) Beyond the angle of repose: a review and synthesis of landslide processes in response to rapid uplift, Eel River, Northern California [Review]. Geomorphology 236:109–131. https://doi.org/10.1016/j.geomorph.2015.02.013

Santangelo M, Gioia D, Cardinali M, Guzzetti F, Schiattarella M (2013) Interplay between mass movement and fluvial network organization: an example from southern Apennines. Italy Geomorphology 188:54–67. https://doi.org/10.1016/j.geomorph.2012.12.008

Santangelo M, Gioia D, Cardinali M, Guzzetti F, Schiattarella M (2014) Landslide inventory map of the upper Sinni River valley, Southern Italy. J Maps. https://doi.org/10.1080/17445647.2014.949313

Schiattarella M, Di Leo P, Beneduce P, Giano SI (2003) Quaternary uplift vs tectonic loading: a case study from the Lucanian Apennine, Southern Italy. Quatern Int 101–102(1):239–251

Schiattarella M, Giano SI, Gioia D (2017) Long-term geomorphological evolution of the axial zone of the Campania-Lucania Apennine, Southern Italy: a review. Geol Carpath 68(1):57–67. https://doi.org/10.1515/geoca-2017-0005

Schiattarella M, Giannandrea P, Corrado G, Gioia D (2024) Landscape planning-addressed regional-scale mapping of geolithological units: an example from Southern Italy. J Maps. https://doi.org/10.1080/17445647.2024.2303335

Schwanghart W, Scherler D (2014) Short communication: TopoToolbox 2 – MATLAB-based software for topographic analysis and modeling in Earth surface sciences. Earth Surf Dynam 2(1):1–7. https://doi.org/10.5194/esurf-2-1-2014

Spalluto L, Fiore A, Miccoli MN, Parise M (2021) Activity maps of multi-source mudslides from the Daunia Apennines (Apulia, Southern Italy). Nat Hazards 106(1):277–301. https://doi.org/10.1007/s11069-020-04461-3

Tarquini S, Vinci S, Favalli M, Doumaz F, Fornaciai A, Nannipieri L (2012) Release of a 10-m-resolution DEM for the Italian territory: comparison with global-coverage DEMs and anaglyph-mode exploration via the web. Comput Geosci 38(1):168–170. https://doi.org/10.1016/j.cageo.2011.04.018

Trigila A, Iadanza C, Spizzichino D (2010) Quality assessment of the Italian landslide inventory using GIS processing. Landslides 7(4):455–470. https://doi.org/10.1007/s10346-010-0213-0

Valente E, Buscher JT, Jourdan F, Petrosino P, Reddy SM, Tavani S, Corradetti A, Ascione A (2019) Constraining mountain front tectonic activity in extensional setting from geomorphology and Quaternary stratigraphy: a case study from the Matese ridge, southern Apennines . Q Sci Rev 219:47–67. https://doi.org/10.1016/j.quascirev.2019.07.001

Whipple KX (2004) Bedrock rivers and the geomorphology of active orogens. Annu Rev Earth Planet Sci 32(1):151–185. https://doi.org/10.1146/annurev.earth.32.101802.120356

Whipple KX, Tucker GE (1999) Dynamics of the stream-power river incision model: implications for height limits of mountain ranges, landscape response timescales, and research needs. J Geophys Research: Solid Earth 104(B8):17661–17674. https://doi.org/10.1029/1999JB900120

Willett SD, McCoy SW, Perron JT, Goren L, Chen C-Y (2014) Dynamic reorganization of River Basins. Science 343(6175):1248765. https://doi.org/10.1126/science.1248765

WP/WLI (1993) A suggested method for describing the activity of a landslide. Bull Int Association Eng Geol 47:53–57